

Five years of operation of the Chandra X-Ray Observatory

Martin C. Weisskopf

Space Sciences Department, NASA/Marshall Space Flight Center

ABSTRACT

The on-orbit performance of the Chandra X-ray Observatory over its first five years of operation is reviewed. The Observatory is running smoothly and the scientific return continues to be outstanding.

Keywords: X-ray imaging, grazing-incidence optics, X-ray astronomy.

1. INTRODUCTION

The Chandra X-ray Observatory is the X-ray component of NASA's Great Observatory Program, which, in addition to Chandra, comprises the Hubble Space telescope and the Spitzer Infrared Telescope Facility. The Chandra X-ray Observatory provides scientific data to the international astronomical community in response to proposals for its use. Data becomes public at most one year after the observation. The Observatory is the result of the efforts of many organizations in the United States and Europe. NASA's Marshall Space Flight Center (MSFC) manages the Project and provides Project Science; NGST (formerly TRW) with the help of many outstanding subcontractors served as prime contractor responsible for providing the spacecraft, the telescope, and assembling and testing the observatory; and the Smithsonian Astrophysical Observatory (SAO) provides technical support and is responsible for ground operations including the Chandra X-ray Center (CXC).

2. THE OBSERVATORY

In 1977, NASA/MSFC and SAO began the study leading to the definition of the then named Advanced X-ray Astrophysics Facility mission. This study, in turn, had been initiated as a result of an unsolicited proposal submitted to NASA in 1976 by Prof. R. Giacconi – Principal Investigator (Harvard University and SAO), and Dr. H. Tananbaum – Co-Principal Investigator (SAO). During the intervening years the project, then referred to as the Advanced X-ray Astrophysics Facility or AXAF, received the highest recommendation by the National Academy of Sciences Astronomy Survey Committee, the flight instruments were selected in response to a NASA Announcement of Opportunity, the Prime Contract was selected in response to a NASA Request for Proposals, the Project demonstrated the ability to build X-ray optics of the requisite quality and specifications, the mission was significantly restructured removing servicing as an option, the name was selected honoring Nobel Prize winner Subramanyan Chandrasekhar, and the Observatory was launched. In 2002, Prof. Giacconi, shown in Figure 1, was awarded the Nobel Prize for his pioneering work in X-ray astronomy.



Figure 1. Professor Riccardo Giacconi (left) receiving the Nobel prize in Physics.

After two attempts earlier in the week, the launch took place on July 23, 1999 using the Space Shuttle Columbia. The Commander was Col. Eileen Collins, the first female commander of a Shuttle flight. With a second rocket system, the Inertial Upper Stage (IUS) attached, the Observatory was both the largest and the heaviest payload ever launched by, and deployed from, a Space Shuttle. Once deployed, and after separating from the IUS, the flight system illustrated in Figure 2 is 13.8-m (43.5-ft) long by 4.2-m (14-ft) diameter, with a 19.5-m (64-ft) solar-panel wingspan. With extensive use of graphite-epoxy structures, the mass is 4,800 kg (10,600 pounds), much of which is in the X-ray optics.

The IUS performed two firings and separated from the Observatory. Finally, after five firings of an internal propulsion system - the last of which took place 15 days after launch - the Observatory was placed in its highly elliptical orbit. This orbit has a nominal apogee of 140,000 km and a nominal perigee of 10,000 km. The inclination to the equator is 28.5° and the satellite is above the radiation belts for more than about 75% of the 63.5-hour orbital period.

The spacecraft is conventional except for its lightweight construction, which utilized primarily composite materials. The spacecraft provides pointing control, power, command and data management, thermal control, and other such services to the scientific payload. The principal elements of the payload are the X-ray telescope, the scientific instruments, and the aspect system used to determine where the observatory was pointed.

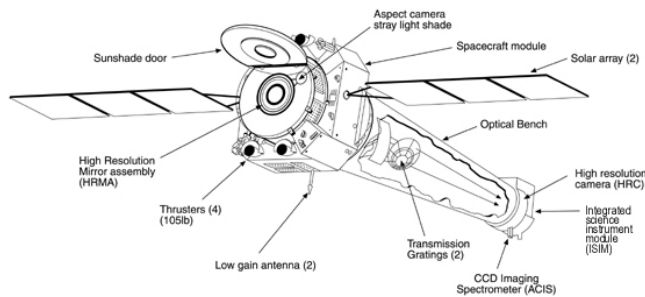


Figure 2. The Chandra X-ray Observatory.

The specified design life of the mission was 3 years with a goal of 5; however, the only perishable (gas for maneuvering) is sized to allow operation for more than 10 years and NASA has officially recognized a 10-year mission. The orbit will be stable for decades.

3. USAGE AND EFFICIENCY

The observing efficiency is dominated by the time spent in the radiation belts at altitudes below about 60,000 km. Other impacts are solar activity, maneuver time, etc. Figure 3 summarizes the efficiency over one year of operations.

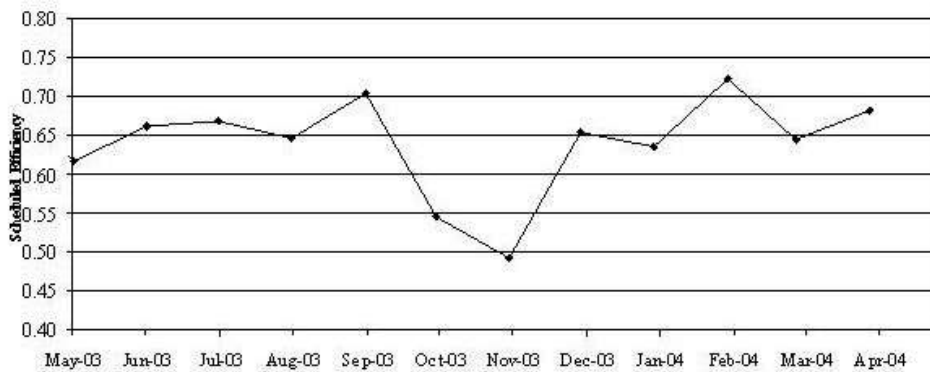


Figure 3. Observing efficiency (time on target) for one year of operation.

The CXC has recently received proposals in response to the sixth announcement of opportunity and the review took place just after this paper was submitted. There were 785 proposals with Principal Investigators from 21 countries. Figure 4 shows the distribution by country. In addition to standard observing proposals there were also 14 Very Large Projects

(those that require more than 1000 ksec to perform), 54 Large Projects (those that require 300 ksec or more), 71 proposals to use the Chandra archives, and 40 proposals to perform theoretical research that has direct impact on the analysis and interpretation of Chandra data. Typically the peer review will accept about 200 observing proposals of which 2 to 3 will be very large projects, and 4-8 will be large projects. In addition, about 15 archive and 15 theory proposals may be accepted.

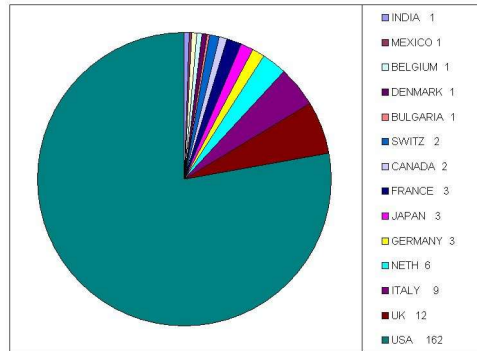


Figure 4. Country of origin of the Chandra Principal Investigators for observing cycle 6.

4. FIRST OBSERVATIONS

The first X-rays focused by the telescope were observed on August 12, 1999 and Figure 5 shows the historic first image. The brightest source in this field we have nicknamed “Leon X-1” in honor of the momentous contributions to the Chandra Project made by the late Leon Van Speybroeck, the Chandra Telescope Scientist. We have identified this source with a 17-th magnitude active galactic nucleus at a redshift of 0.32.¹

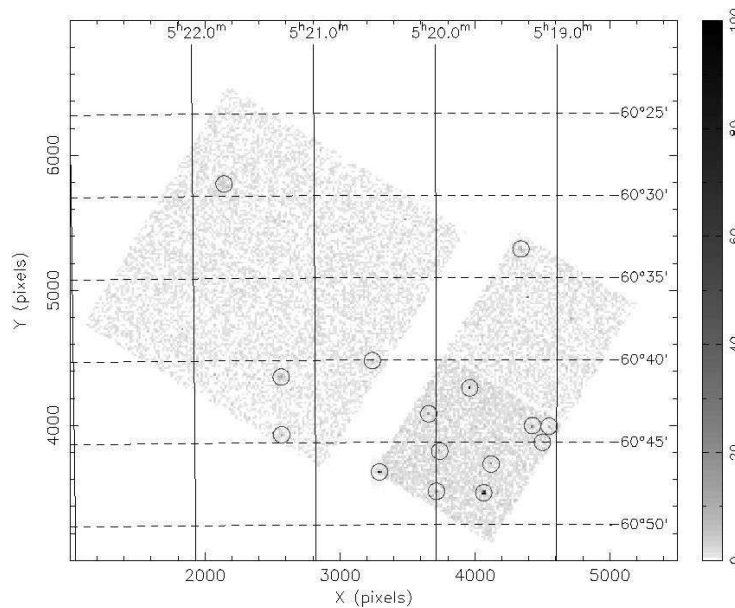


Figure 5. The first Chandra Field. “Leon X-1” is the bright source at X = 4065, Y = 3500.

Figure 6 shows one of the most famous early images. This image of the Crab Nebula and its pulsar revealed an exciting new discovery²- the bright inner elliptical ring showing the first direct observation of the shock front where the wind of particles from the pulsar begins to radiate in X-rays via the synchrotron process. Discoveries of new astronomical features in Chandra images have been the rule, not the exception. Recently, using Chandra one has been able, for the first time, to study the Crab’s pulsed spectrum at all pulse phases.³

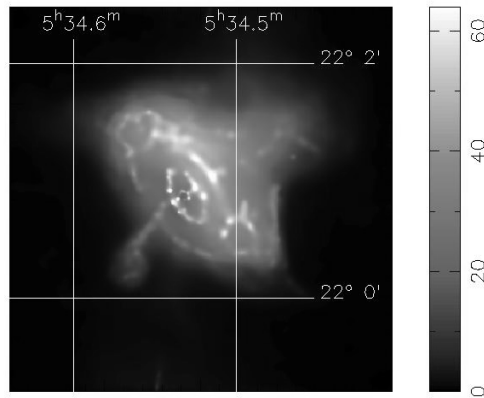


Figure 6. Chandra image of the Crab Nebula.

5. INSTRUMENTATION

The Chandra optics and detectors have provided, for the first time, sub-arcsecond imaging, sub-arcsecond spectrometric imaging, and, together with transmission gratings, high-resolution X-ray spectroscopy. With these capabilities, a wide variety of high-energy phenomena in a broad range of astronomical objects are being observed. The telescope is made of four concentric, precision-figured, superpolished Wolter-1 X-ray telescopes, similar to those used for both the Einstein⁴ and Rosat⁵ observatories, but of much higher quality, larger diameter, and longer focal length. The Wolter-1 design uses a paraboloid of revolution followed by a hyperboloid of revolution. Two reflections minimize coma. The 4-mirror-pair grazing-incidence optic is constructed of Zerodur, a glassy ceramic chosen for its high thermal stability. The mirrors are coated with iridium, chosen for high reflectivity at the X-ray energies of interest, 0.08 – 10.0-keV (15-0.12 nm).

The aspect camera system includes a visible-light telescope and CCD camera in a housing coaligned with, and attached to, the X-ray telescope. A fiducial-light transfer system is used to project lights attached to the focal-plane instruments onto the aspect camera. Thus, the aspect camera simultaneously determines both where the observatory was pointing and the location of the X-ray detector positions relative to the pointing direction. The aspect solution's accuracy depends on the number of stars detected in the field, but is typically 0.6 seconds of arc. In many observations the astrometry may be improved through the identification of X-ray sources with counterparts in other wavelength bands.

The science instrument module includes mechanisms for focusing and translating the focal-plane instruments. Translation of the instruments is required as X-ray beam-splitters are not very efficient.

Just behind the telescope are 2 objective transmission gratings - the Low-Energy Transmission Grating⁶ (LETG), optimized for longer X-ray wavelengths and the High-Energy Transmission Grating⁷ (HETG), optimized for shorter wavelengths. Positioning mechanisms allow one to insert, by command, either grating into the converging beam to disperse the x-radiation onto the focal plane producing high-resolution spectra read-out by one of the detectors. Figure 7 illustrates the concept and the placement for the HETG. The LETG is similar in to the HETG except that all the facets are identical and are optimized for longer wavelengths. The gratings allow for measurements with spectral resolving power of $\lambda/\Delta\lambda = E/\Delta E > 500$ for wavelengths of > 0.4 -nm (energies < 3 keV).

The Space Research Institute of the Netherlands and the Max-Planck-Institut für Extraterrestrische Physik designed and fabricated the LETG. The assembly is made of 540 grating facets with gold bars of 991-nm period. The LETG provides high-resolution spectroscopy from 0.08 to 2 keV (15 to 0.6 nm).

The Massachusetts Institute of Technology (MIT) designed and fabricated the High-Energy Transmission Grating (HETG). The HETG uses 2 types of grating facets - the Medium-Energy Gratings (MEG) which, when inserted, are placed behind the telescope's 2 outermost shells, and the High-Energy Gratings (HEG), behind the 2 innermost shells. The HEG and MEG are oriented at slightly different dispersion directions. With polyimide-supported gold bars of 400-nm and 200-nm periods, the HETG provides high-resolution spectroscopy from 0.4 to 4 keV (MEG, 3 to 0.3 nm) and from 0.8 to 8 keV (HEG, 1.5 to 0.15 nm).

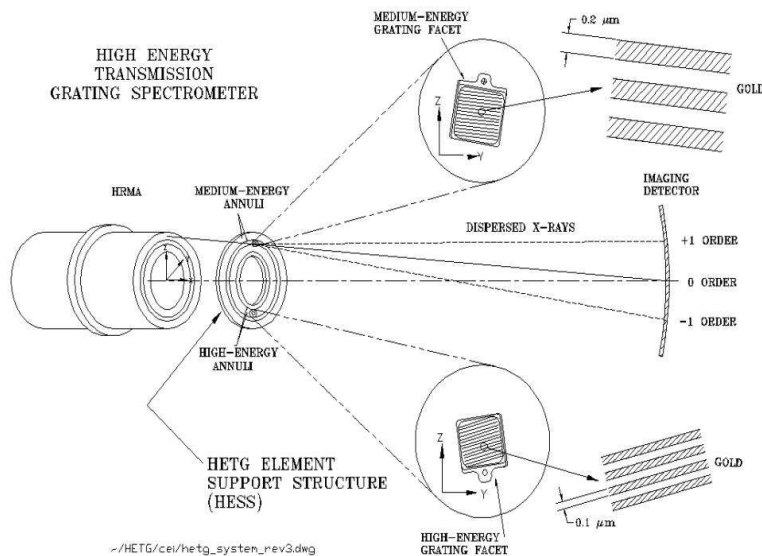


Figure 7. Grating layout.

Chandra's two focal-plane science instruments are the High Resolution Camera⁸ (HRC) and the Advanced CCD Imaging Spectrometer (ACIS)⁹. SAO designed and fabricated the HRC. One of the HRC detectors is made of a 10-cm-square microchannel plate, and provides high-resolution imaging over a 31-arcmin-square field of view. A second detector, comprising 3 rectangular segments (3-cm-by-10-cm each) mounted end-to-end along the grating dispersion direction, serves as the primary readout detector for the LETG. Both of the HRC detectors are coated with a cesium-iodide photocathode and have thin aluminized polyimide shields to prevent contamination by ions and ultraviolet light.

The Pennsylvania State University MIT built the Advanced CCD Imaging System (ACIS) with charge-coupled devices (CCDs) fabricated by MIT's Lincoln Laboratory. As with the HRC, there are two detector systems. One is made of a 2-by-2 array of CCDs, and provides high-resolution spectrometric imaging over a 17-arcmin-square field of view. The other, a 6-by-1 array mounted along the grating dispersion direction, serves as the primary readout detector for the HETG. Two types of CCDs were used, 8 front-illuminated (FI) and two back-illuminated (BI). The latter CCDs have higher efficiency at lower energies than the FI devices, but were much more difficult to fabricate. One BI CCD was placed at the on-axis focal position of the 6 x 1 array. Thus this particular CCD also provides high-resolution spectrometric imaging extending to lower energies, but over a smaller (8-arcmin-square) field than the 2 x 2 array. Both ACIS detector systems have thin aluminized polyimide filters to minimize contamination by visible light.

Despite successful science operations, the Observatory has had to deal with some technical difficulties that have had their impact on scientific performance. The front- (not the back-) illuminated ACIS CCDs suffered damage, which increased the charge transfer inefficiency, as a result of bombardment by low energy (100 keV) protons crudely focused by the telescope by means of Rutherford scattering as the Observatory entered the radiation belts. Following a procedure of removing ACIS from the focal plane during radiation belt passages has dramatically minimized subsequent increases in the charge transfer inefficiency. O'Dell et al.¹⁰ discuss the Chandra approach to radiation management.

Both ACIS filters, which are close to the CCDs and therefore the coldest (120 °C) surfaces on the observatory, are collecting hydrocarbon contamination at the rate of about one-half an optical depth at the Carbon k-edge per year. Figure 8 shows the buildup as a change in the optical depth to the Manganese-L complex at about 0.7 keV. Marshall et al.¹¹ have discussed the composition of the contaminant in some detail. Plucinsky et al. give an update elsewhere in these proceedings. Prior to launch the plan had been to bake off the expected contamination after a nominal amount of buildup and the ACIS instrument was designed, and repeatedly tested, to accomplish this. Use of bakout was, however, complicated subsequent to launch by the potential negative impact on the charge transfer efficiency of the CCDs. It was discovered that these appear to suffer an increase in charge transfer inefficiency (and thus an increase in energy resolution) as a consequence of a bakeout performed to remove charge traps produced by the proton damage discussed above. The increase is attributed to the migration of charge traps created by the low energy protons – reverse annealing. We are

performing detailed tests and studies to determine an effective bakeout strategy. Of course there is hardly any impact on much of the Chandra science, at least at energies above 1 keV.

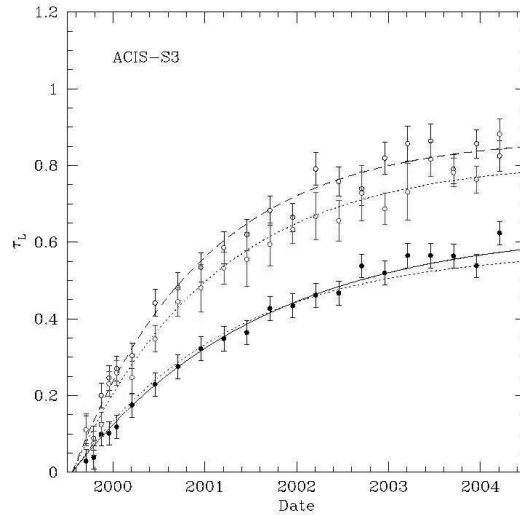


Figure 8. Optical depth of the contaminant on the ACIS filter over the spectroscopy array versus time based on measurements at the Manganese-L edge. The two upper curves are for the opposite edges of the filter in the long direction whereas the lower curve is representative of the center of the filter. The increased optical depth at the edges tracks the temperature gradient. Figure kindly provided by A. Vikhlinin (CXC).

Point Spread Function

The Observatory's point spread function, as measured during ground calibration, had a full width at half-maximum under 0.5 arcsec and a half-power diameter under 1 arcsec. The pre-launch prediction for the on-orbit encircled-energy fraction was that a 1-arcsec-diameter circle would enclose at least half the flux from a point source. A relatively mild dependence on energy, resulting from diffractive scattering by surface microroughness, attests to the 3 angstroms rms surface roughness. The ground measurements were taken under environmental conditions different than those encountered on-orbit. The effects of gravity and the finite distance and the size of the various X-ray sources used were unique to the ground calibration. On-orbit the performance includes the spatial resolution of the flight detectors and uncertainties in the aspect solution. The on-orbit performance met expectations as illustrated in Figure 9.

The tremendous advancement in angular resolution that the Chandra optics provides introduces new considerations for the analysis of the data. An example is that now, for very bright sources, one has to account for the energy dependence of the flux scattered out of the beam by the interstellar medium.

The Observatory's capability for high-resolution imaging enables detailed high-resolution studies of the structure of extended X-ray sources, including supernova remnants, astrophysical jets, and hot gas in galaxies and clusters of galaxies. The additional capability for spectrometric imaging allows studies of structure, not only in X-ray intensity, but also in temperature and in chemical composition. Through these observations, users are addressing several of the most exciting topics in contemporary astrophysics.

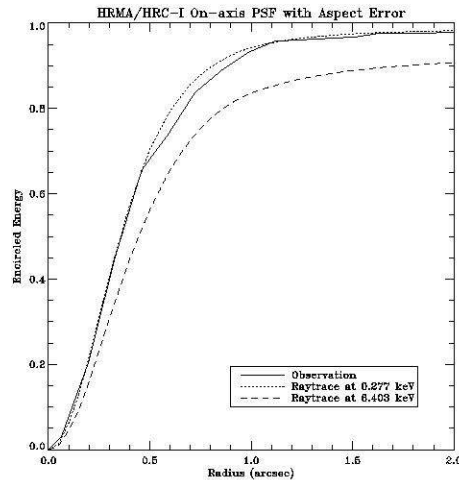


Figure 9. Encircled energy versus radius comparing pre-launch predictions at two energies to on-orbit performance.

In addition to mapping the structure of extended sources, the high angular resolution permits studies of discrete sources, which would otherwise be impossible. In example is shown in Figure 10 where one sees X-rays produced by TWA 5B, a brown dwarf orbiting a young binary star system known as TWA 5A¹². This observation was for addressing the question as to how do brown dwarfs heat their upper atmospheres, or coronas, to X-ray-emitting temperatures of a few million degrees.

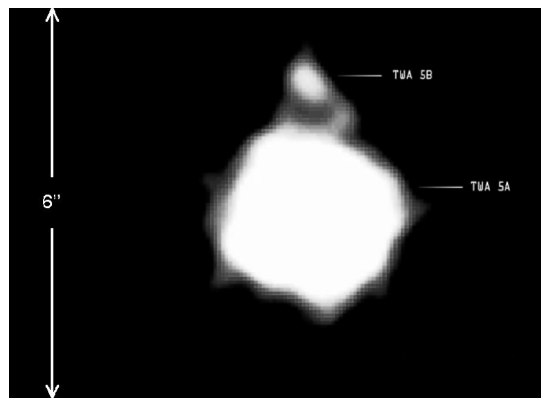


Figure 10. X-rays produced by TWA 5B, a brown dwarf orbiting a young binary star system known as TWA 5A. Courtesy of NASA/CXC/Chuo U.¹³

Equally important are Chandra's unique contributions to high-resolution dispersive spectroscopy. As the capability for visible-light spectroscopy initiated the field of astrophysics about a century ago, high-resolution X-ray spectroscopy now contributes profoundly to the understanding of the physical processes in cosmic X-ray sources and is the essential tool for diagnosing conditions in hot plasmas. The high spectral resolution of the Chandra gratings isolates individual lines from the myriad of spectral lines, which would overlap at lower resolution.

6. RECENT DISCOVERIES

From planetary systems to deep surveys of the faintest and most distant objects, the scientific results from the first five years of Chandra operations have been exciting and outstanding. We conclude this overview with a series of images illustrating recent results. We begin with images of the X-ray emission from the planet Saturn.¹⁴ Figure 11 shows that the emission is concentrated in the equator. Additional images taken by Elsner and Waite¹⁵ show that the emission pattern is more complex and varies with time.

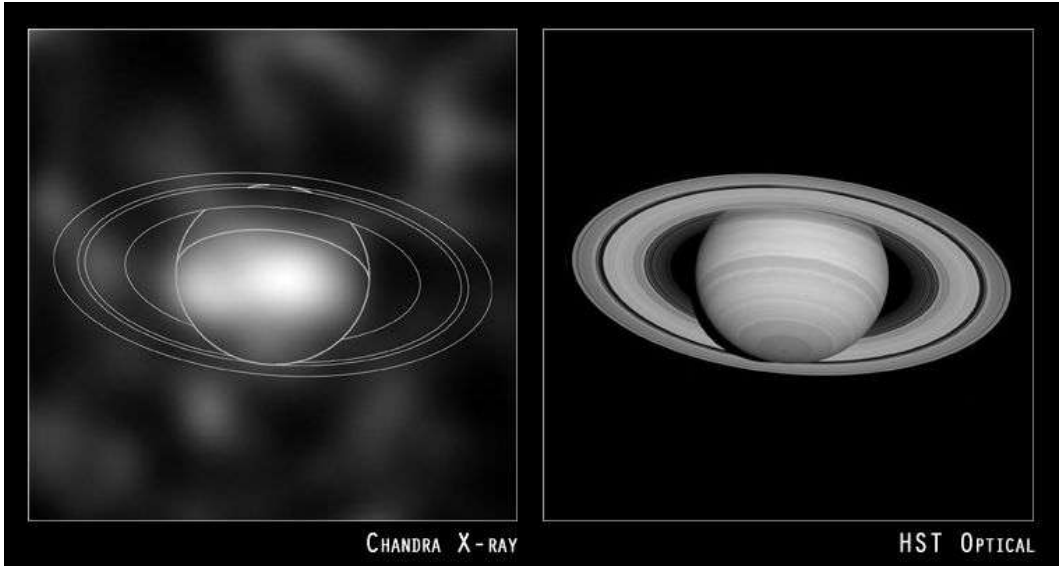


Figure 11: X-ray and optical images of Saturn. X-ray: NASA/U. Hamburg/J.Ness et al; Optical: NASA/STScI.

One of the more challenging images to obtain is shown in Figure 12. These data of Titan, Saturn’s largest moon, were taken on January 5, 2003 when Titan, the only moon in the solar system with a thick atmosphere, crossed in front of the Crab Nebula. Titan's transit of the Nebula enabled Chandra to image the X-ray shadow. In turn, the diameter of the shadow was used to measure height of the of the X-ray absorbing region of Titan's atmosphere.¹⁶

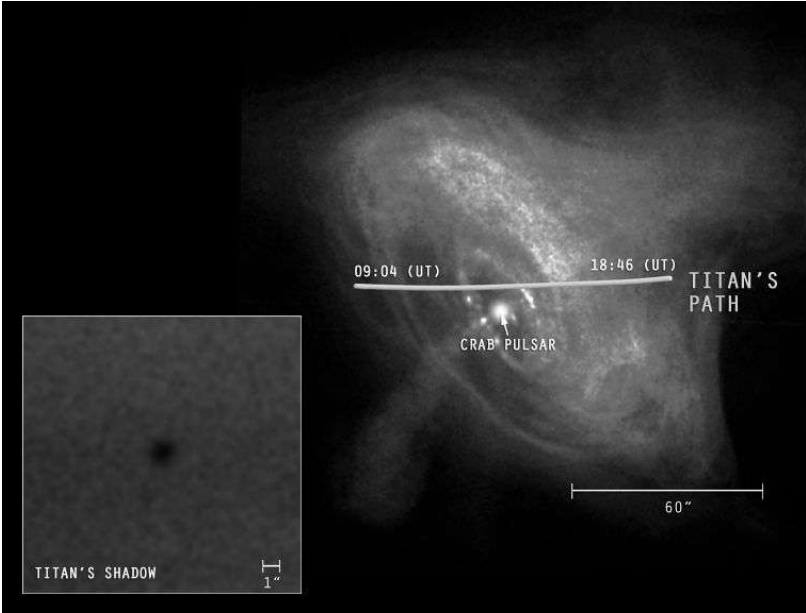


Figure 12. Chandra image of Titan’s shadow (inset) while passing in front of the Crab Nebula. NASA/CXC/Penn State/K.Mori et al.

Perhaps one of the most spectacular Chandra images is the one of the center of our own galaxy¹⁷ shown in Figure 13. Here one sees the presence of both point-like discrete sources (over 1000) and diffuse extended emission. The large amounts of

hot gas has been heated and chemically enriched by numerous stellar explosions. Detailed studies, including follow up observations in other wavelength bands, are in progress and should have much to say concerning not only the population of compact, X-ray-emitting, objects in the Galaxy but also the history of the state of activity of the central black hole.

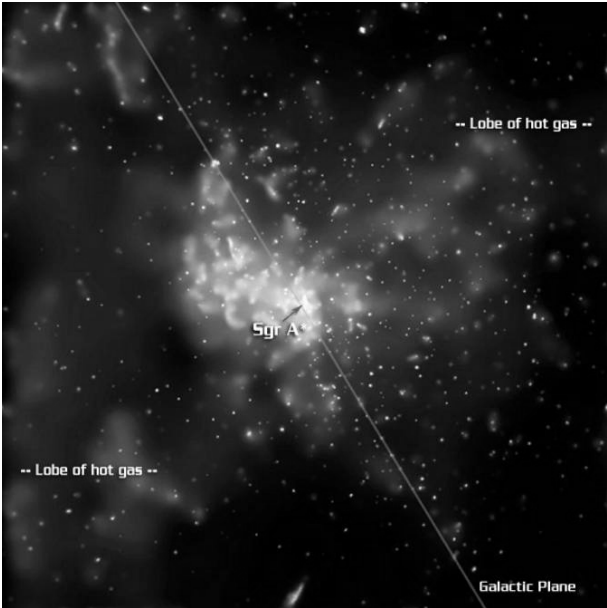


Figure 13. Image of the Galactic Center. The image is 8.4 arcmin on a side. Courtesy NASA / CXC/ MIT/ F.K.Baganoff et al.

The final legacy of Chandra may ultimately be led by the spectroscopic data. The energy resolution, enabled by the quality of the optics, is providing new and extremely complex results. For example, high-resolution spectra of Seyfert galaxies are providing new details about the physical and dynamical properties of material surrounding the active nucleus. In the case of Seyfert 1s, whose signal is dominated by a bright X-ray continuum from the central engine, the partially ionized circum-source material introduces prominent patterns of absorption lines and edges. Figure 14, e.g. shows a LETG/HRC spectrum of NGC 5548 with its dozens of absorption lines clearly evident.¹⁸

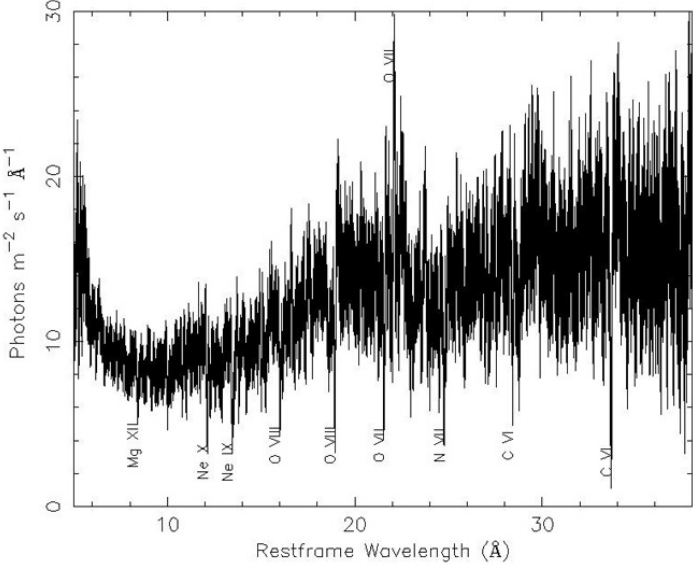


Figure 14. LETG/HRC spectrum of the Seyfert 1 galaxy NGC 5548.¹⁴ Several prominent absorption lines from H-like and He-like ions are marked, as is the forbidden line of He-like oxygen.

For Seyfert 2's the strong continuum from the central engine is not seen directly, so the surrounding regions are seen in emission. Figure 15 provides an example through a LETG/HRC observation of NGC 1068.

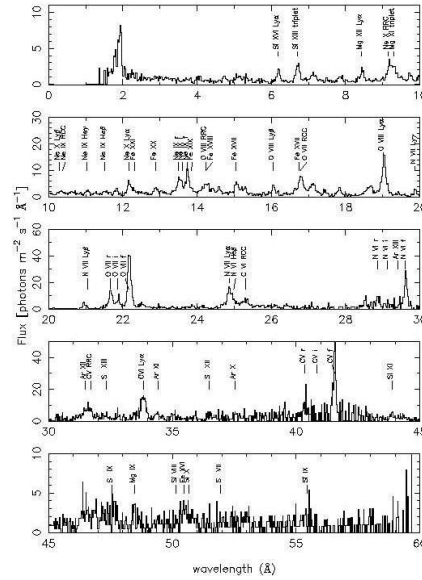


Figure 15. Emission-line spectrum from the Seyfert 2 galaxy NGC 1068.¹⁹ Kindly provided by A. Kinkhabwala .

X-ray flashes resemble a lower energy and longer-duration version of a gamma-ray burst and their properties led to the speculation that they were gamma-ray bursts that occurred early in the history of the Universe, i.e. at very high redshift.

Figure 16, however, shows the results²⁰ of utilizing the accurate Chandra positions of the X-ray afterglows from two X-ray flashes to discriminate possible optical counterparts found with HST. The images associate the afterglows with blue star-forming galaxies at redshifts less than 3.5 and therefore cannot be due to gamma-ray bursts at very high redshift.

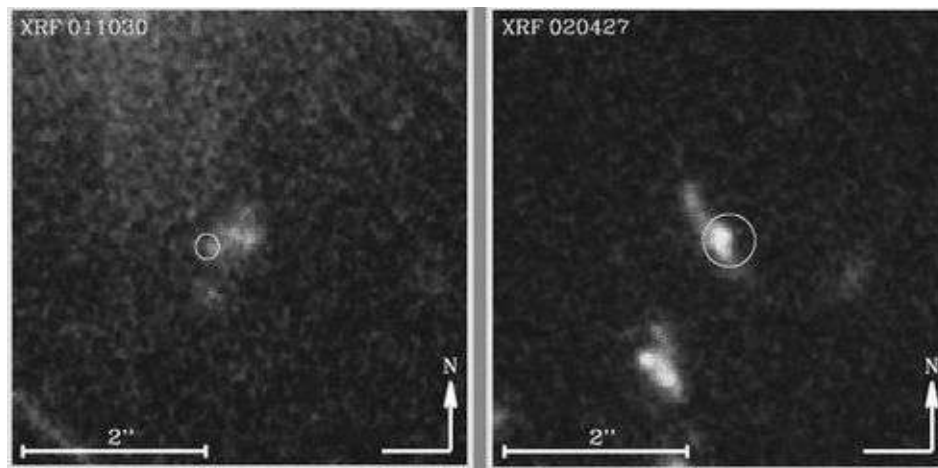


Figure 16. HST images with error circles based on the X-ray positions. Courtesy (NASA/P. van Dokkum (Yale) & J. Bloom (CfA))

One of the more important triumphs of the Observatory has been to use the angular resolution and high sensitivity to perform detailed surveys of extended objects such as globular clusters, galaxies, and clusters of galaxies. Figure 17 shows 4 recent deep exposures²¹ of the nearby face-on spiral galaxy NGC 1637. Seventy-nine point-like X-ray sources were detected and, as the time lapsed images showed, many exhibited a high degree of variability. Together with HST images, it was possible to identify an optical counterpart for an ultraluminous source – the middle source in the row of three in the lower left image in Figure 17. Ultraluminous X-ray sources radiate above the Eddington limit for a solar mass compact object and are speculated to be intermediate mass black holes.

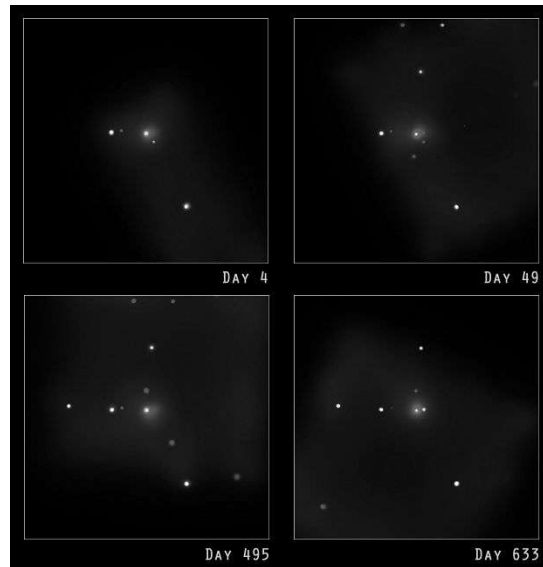


Figure 17. Four images of NGC 1637. Courtesy NASA/CXC/Penn State/S. Immler et al. Each panel is 8.5 arcmin per side.

In Figure 18 we show a recent Chandra composite image of the giant elliptical galaxy M87. A central jet is surrounded by nearby bright arcs and dark cavities in the multimillion-degree hot gas. Much further out, at a distance of about fifty thousand light years from the galaxy's center, faint rings can be seen and two spectacular plumes extend beyond the rings. These features, together with radio observations, are dramatic evidence that repetitive outbursts from the central supermassive black hole have been affecting the entire galaxy for a hundred million years or more

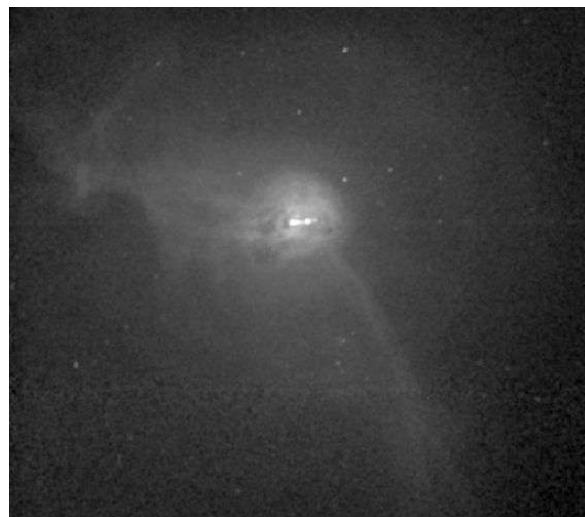


Figure 18. Deep exposure of M87. (The faint horizontal streaks are instrumental artifacts - trailed images as the CCDs are read out).
NASA/CXC/W. Forman et al.

Chandra observations of clusters of galaxies frequently exhibit previously undetected structures with characteristic angular scales of a few arc seconds. These include “bubbles” where there is strong radio emission, bow shocks, and cold fronts. Such phenomena are illustrated in Figures 19, 20, and 21. Figure 19 of the Perseus cluster²² is a spectacular example of bubbles produced in regions where there is strong radio emission. The image is based on a 53-hour Chandra observation of the central region of the cluster and has also revealed wavelike features that appear to be sound waves. The features were discovered by using an image-processing technique to bring out subtle changes in brightness. These sound waves may have been produced by explosive events occurring around the central supermassive black hole in Perseus A, the large galaxy at the center of the cluster. The detection of the sound waves may solve the long-standing mystery of why the hot gas in the central regions of the Perseus cluster has not cooled over the past ten billion years to form trillions of stars. As sound waves move through gas, they are eventually absorbed and their energy is converted to heat. In this way, the sound waves from the supermassive black hole in Perseus A could keep the cluster gas hot. We note that a major triumph of Chandra (and XMM-Newton) high-resolution spectroscopic observations has been the discovery that that gas in the clusters is typically not cooling to below about 1-2 keV.²³

Figure 20 shows a bow shock propagating in front of a bullet-like gas cloud just exiting a disrupted cluster core. This observation of the galaxy cluster 1E0657-56 is the first clear example of such a shock front.²⁴ In contrast, Figure 21 of Abell 2152²⁵ is an example of a shockless cold front.

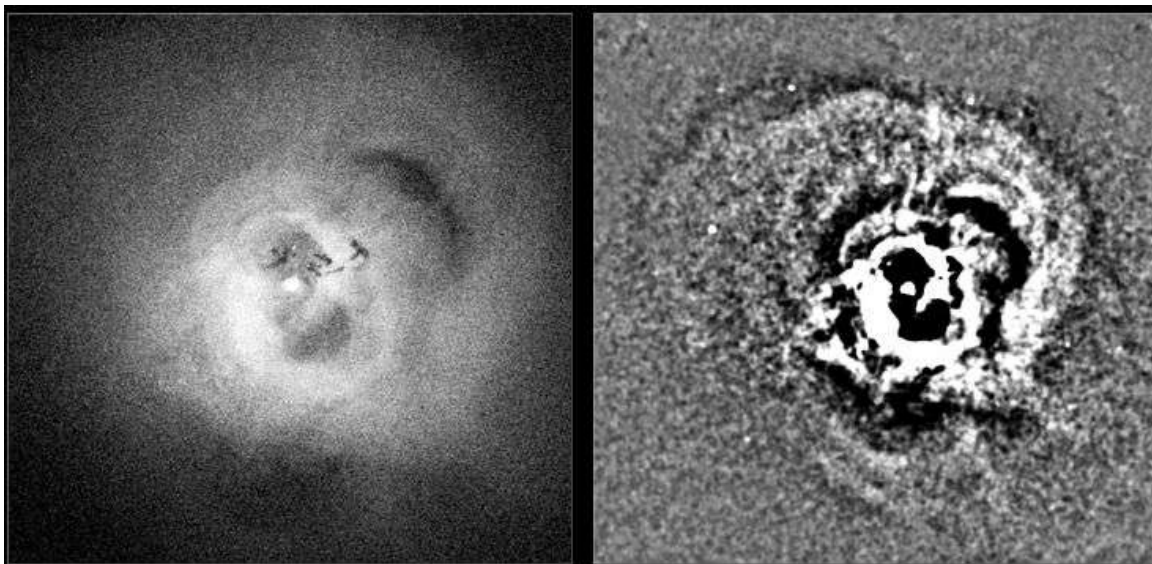


Figure 19. X-ray core of the Perseus cluster. Courtesy NASA/IOA/A. Fabian et al.

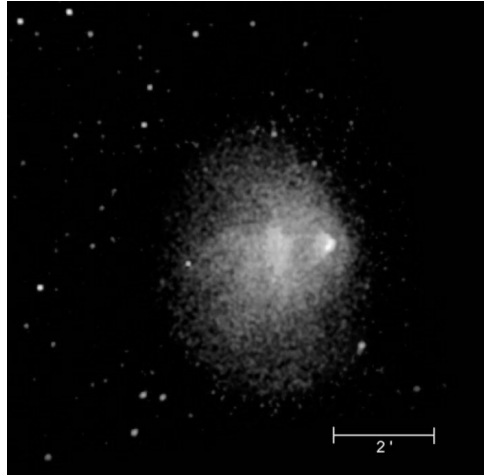


Figure 20. The Chandra image of the merging, hot galaxy cluster 1E 0657-56. Courtesy NASA/SAO/CXC/M.Markevitch et al.

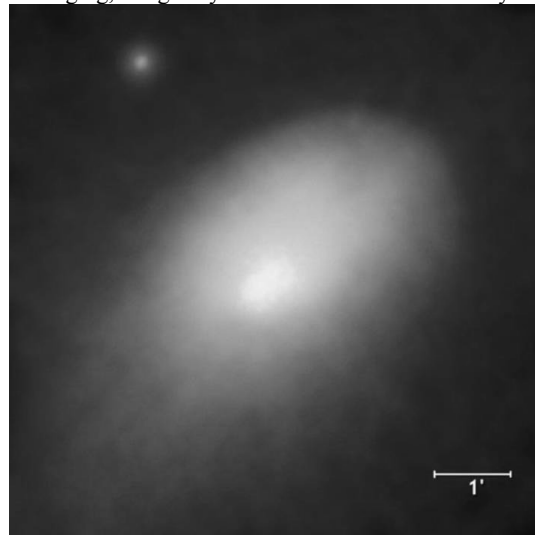


Figure 21. Chandra Image of the galaxy cluster Abell 2142. The sharp border to the top right is an example of a cold front. Courtesy NASA/CXC/SAO.

The study of active galaxies is one of the centerpieces of studies with Chandra. Figure 22 shows images of double quasar nuclei identified as such based on their X-ray characteristics. NGC 6240 was the first such detected²⁶ and is a butterfly-shaped galaxy that is the product of the collision of two smaller galaxies. In another Chandra observation, the quasar pair Q2345+007 A and B

was thought to be an apparent double due to gravitational lensing by an intervening mass. However no intervening galaxy or cluster had been found, leading to a speculation that the dual image might be caused by a new type of cluster that contains hot gas and dark matter, but no stars. Such a “dark cluster” would be invisible to optical and ultraviolet telescopes, but would be detectable in X-rays. The Chandra X-ray image²⁷ however, shows no evidence for a massive dark cluster and the X-ray spectra of the two quasars were distinctly different, supporting the conclusion that they are in fact distinct objects.

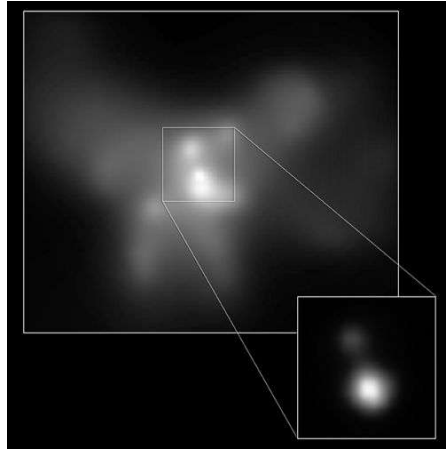


Figure 22. The Chandra image of NGC 6240. Full field is $.35 \times .3$ arcmin and the inset is 4 arcsec per side.
Courtesy NASA/CXC/MPE/S.Komossa et al.

No discussion of data taken with the Observatory is complete without a mention of the deep Chandra Surveys. These are deep exposures of particular regions of the sky to study the populations of the objects detected, especially the faintest ones. This work is an outgrowth of the study the diffuse X-ray background, the nature of which had been a puzzle for nearly 40 years, although the lack of distortion of the spectrum of the Cosmic Microwave Background placed a strong upper limit to the possibility of a truly diffuse component.²⁸ Observations with ROSAT at energies below 2 keV made a major step in resolving a significant fraction (70-80%) into discrete objects.²⁹ Currently two long exposures have been accomplished with the Chandra X-ray Observatory - the Chandra Deep Fields North³⁰ depicted in Figure 23 with 2 Ms of exposure, and the Chandra deep field south³¹ with 1 Msec. These surveys have extended the study of the background to flux levels more than an order of magnitude fainter than previously in the 0.5-2.0 keV band and have resolved over 90% of the background into a variety of discrete sources. The largest uncertainty in establishing the fraction is now in the knowledge of the total level of the background itself. This past year an additional Ms was devoted to the Chandra deep field north and we can be sure that the extended survey will provide new and exciting astrophysical insights.

Finally, observations with Chandra have begun to have an impact on our understanding of cosmology. Recent examples include the study of the dark matter distribution through observation of the hot, X-ray-emitting gas in Abell 2029, which concluded that standard cold dark matter models best fit the observations.³² Elsewhere, adopting the reasonable hypothesis that the ratio of baryonic to dark matter in clusters should be a constant, Chandra observations of 26 clusters were used³³ to provide a measure of cosmological parameters independent of, but in agreement with, results based on the observations of type 1 supernovae and the microwave background. Combining all these data provides further constraints on cosmological models and we may expect new insights in the years to come.

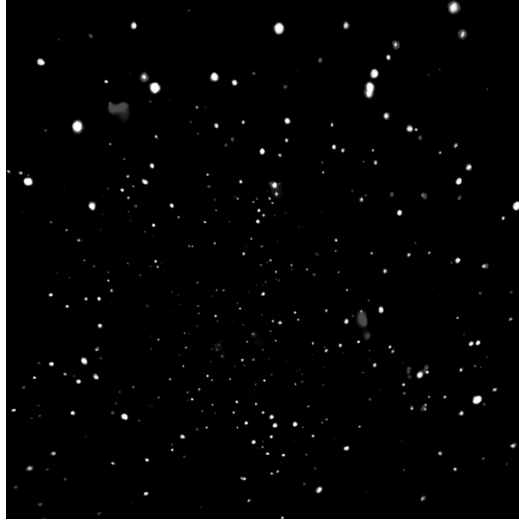


Figure 23. Two-million-second image of the Chandra Deep Field North. Courtesy NASA/CXC/PSU/D.M.Alexander, F.E.Bauer, W.N.Brandt et al.

7. WORLD-WIDE WEB SITES

<http://chandra.harvard.edu/>: Chandra X-ray Center (CXC), operated for NASA by the Smithsonian Astrophysical Observatory.

<http://wwwastro.msfc.nasa.gov/xray/axafps.html>: Chandra Project Science, at the NASA Marshall Space Flight Center.

<http://hea-www.harvard.edu/HRC/>: Chandra High-Resolution Camera (HRC) team, at the Smithsonian Astrophysical Observatory (SAO).

<http://www.astro.psu.edu/xray/axaf/axaf.html>: Advanced CCD Imaging Spectrometer (ACIS) team at the Pennsylvania State University (PSU).

<http://acis.mit.edu/>: Advanced CCD Imaging Spectrometer (ACIS) team at the Massachusetts Institute of Technology.

<http://www.sron.nl/missions/Chandra>: Chandra Low-Energy Transmission Grating (LETG) team at the Space Research Institute of the Netherlands.

<http://www.ROSAT.mpe-garching.mpg.de/axaf/>: Chandra Low-Energy Transmission Grating (LETG) team at the Max-Planck Institut für extraterrestrische Physik (MPE).

<http://space.mit.edu/HETG/>: Chandra High-Energy Transmission Grating (HETG) team, at the Massachusetts Institute of Technology.

<http://hea-www.harvard.edu/MST/>: Chandra Mission Support Team (MST), at the Smithsonian Astrophysical Observatory.

<http://ipa.harvard.edu/>: Chandra Operations Control Center, operated for NASA by the Smithsonian Astrophysical Observatory.

<http://ifkki.kernphysik.uni-kiel.de/soho>: EPIN particle detector.

REFERENCES

- ¹ Weisskopf, M.C., Aldcroft, T., Cameron, R. A., Gandhi, P., Foellmi, C., Elsner, R.F., Patel, S.K., & O'Dell, S.L. 2004, submitted to the *Astrophysical Journal*.
- ² Weisskopf, M.C., Hester, J.J., Tennant, A.F., Elsner, R.F., Shultz, N.S., Marshall, H.L., Karovska, M., Nichols, J.S., Swartz, D.A., Kolodziejczak, J.J. & O'Dell, S.L. 2000, *ApJ*, 536, L81.
- ³ Weisskopf, M.C., O'Dell, S.L., Paerels, F., Elsner, R.F., Becker, W., Tennant, A.F., and Swartz, D. 2004, *The Astrophysical Journal*, Volume 601, pp1050-1057.
- ⁴ See for example <http://heasarc.gsfc.nasa.gov/docs/einstein/heao2.html>
- ⁵ See for example <http://wave.xray.mpe.mpg.de/rosat>
- ⁶ See Mendez, M. SPIE, 4851-05 and references therein.
- ⁷ See Flanagan, K. SPIE 4851-04 and references therein.
- ⁸ See Murray, S. S. SPIE 4851-02 and references therein.
- ⁹ See Garmire, G. P. et al. SPIE 4851-03 and references therein.
- ¹⁰ O'Dell, S. et al. 2003, *Proceedings of the SPIE*, Volume 4851, pp. 77-88.
- ¹¹ Marshall, H. L., Tennant, A., Grant, C. E., Hitchcock, A. P., O'Dell, S. L., Plucinsky, P. 2004, *X-ray and Gamma-Ray Instrumentation for Astronomy XIII*. Edited by Flanagan, Kathryn A. and Siegmund, Oswald H. W. *Proceedings of the SPIE*, Volume 5165, pp. 497-508.
- ¹² Tsuboi, Y., Maeda, Y., Feigelson, E. D., Garmire, G. P., Chartas, G., Mori, K., Pravdo, S. H. 2003, *The Astrophysical Journal*, Volume 587, Issue 1, pp. L51-L54.
- ¹³ Pictures that are publicly available at the Chandra web site at <http://chandra.harvard.edu> have credits labeled "Courtesy of". The acronyms may be found at this site.
- ¹⁴ Ness, J. -U., Schmitt, J. H. M. M., Wolk, S. J., Dennerl, K., & Burwitz, V. 2004, *Astronomy and Astrophysics*, Volume 418, pp 337-345.
- ¹⁵ R.F.Elsner 2003, private communication.
- ¹⁶ Mori, K., Tsunemi, H., Katayama, H., Burrows, D. N., Garmire, G. P., Metzger, A. E. 2004, *The Astrophysical Journal*, Volume 607, pp. 1065-1069.
- ¹⁷ Baganoff, F. K., Maeda, Y., Morris, M., Bautz, M. W., Brandt, W. N., Cui, W., Doty, J. P., Feigelson, E. D., Garmire, G. P., Pravdo, S. H., Ricker, G. R., Townsley, L. K., 2003, *The Astrophysical Journal*, Volume 591, Issue 2, pp. 891-915.
- ¹⁸ Kaastra, J. S., Mewe, R., Liedahl, D. A., Komossa, S., and Brinkman, A. C. 2000, *Astronomy and Astrophysics*, Volume 354, L83.
- ¹⁹ Brinkman, A. C., Kaastra, J. S., van der Meer, R. L. J., Kinkhabwala, A., Behar, E., Paerels, F., Kahn, S. M. and Sako, M. 2002, *Astronomy and Astrophysics*, Volume 396, p.761-772.
- ²⁰ Bloom, J. S., Fox, D., van Dokkum, P. G., Kulkarni, S. R., Berger, E., Djorgovski, S. G., Frail, D. A. 2003, *The Astrophysical Journal*, Volume 599, pp. 957-963.
- ²¹ Immler, S., Wang, Q. D., Leonard, D. C., Schlegel, E. M. 2003, *The Astrophysical Journal*, Volume 595, pp. 727-742.
- ²² Fabian, A. C., Sanders, J. S., Etori, S., Taylor, G. B., Allen, S. W., Crawford, C. S., Iwasawa, K., Johnstone, R. M., and Ogle, P. M. 2000, *MNRAS*, Volume 318, L65
- ²³ See for example the discussion in Fabian, A.C. 2002, "Cooling Flows in Clusters of Galaxies" in *Lighthouses of the Universe: The Most Luminous Celestial Objects and Their Use for Cosmology*, *Proceedings of the MPA/ESO*, p. 24.
- ²⁴ Markevitch, M., Gonzalez, A. H., David, L., Vikhlinin, A., Murray, S., Forman, W., Jones, C., Tucker, W. 2002, *The Astrophysical Journal*, Volume 567, Issue 1, pp. L27-L31.
- ²⁵ Markevitch, M., Ponman, T. J., Nulsen, P. E. J., Bautz, M.W., Burke, D. J., David, L. P., Davis, D., Donnelly, R. H., Forman, W. R., Jones, C., and 12 coauthors, 2000, *The Astrophysical Journal*, Volume 541, Issue 2, pp. 542-549.
- ²⁶ Komossa, S., Burwitz, V., Hasinger, G., Predehl, P., Kaastra, J. S., Ikebe, Y. 2003, *The Astrophysical Journal*, Volume 582, pp. L15-L19
- ²⁷ Green, P. J., Kochanek, C., Siemiginowska, A., Kim, Dong-Woo, Markevitch, M., Silverman, J., Dosaj, A., Jannuzi, B. T. & Smith, C. 2002, *The Astrophysical Journal*, Volume 571, Issue 2, pp. 721-732
- ²⁸ Mather, J. C. et al. 1990, *The Astrophysical Journal*, Volume 354, L4.
- ²⁹ Hasinger, G. et al. 1998, *Astronomy and Astrophysics*, Volume 329, 482.
- ³⁰ Alexander, D. M., Bauer, F. E., Brandt, W. N., Hornschemeier, A. E., Vignali, C., Garmire, G. P., Schneider, D. P., Chartas, G., Gallagher, S. C. 2003, *The Astronomical Journal*, Volume 125, Issue 2, pp. 383-397. And references therein.
- ³¹ Giacconi, R., Rosati, P., Tozzi, P., Nonino, M., Hasinger, G., Norman, C., Bergeron, J., Borgani, S., Gilli, R., Gilmozzi, R., Zheng, W. 2001, *Astrophysical Journal*, Volume 551, 642.
- ³² Lewis, A. D., Buote, D. A., Stocke, J. T. 2003, *The Astrophysical Journal*, Volume 586, pp. 135-142.
- ³³ Allen, S.W., Schmidt, R.W., Ebeling, H., Fabian, A.C., van Speybroeck, L. 2004, *Monthly Notices of the Royal Astronomical Society* (in press).

